

Anisotropic Time-Domain Electronic Response in Cuprates

F. Giusti^{1,2}, A. Montanaro^{1,2}, A. Marciniak^{1,2}, F. Randi³, F. Boschini^{4,5,6}, F. Glerean^{1,2}, G. Jarc^{1,2}, H. Eisaki⁷, M. Greven⁸, A. Damascelli^{4,5}, A. Avella^{9,10}, D. Fausti^{1,2}*

¹ *Department of Physics, Università degli Studi di Trieste, 34127 Trieste, Italy*

² *Elettra Sincrotrone Trieste S.C.p.A., 34127 Basovizza Trieste, Italy*

³ *Joseph Henry Laboratories of Physics, Princeton University, Princeton, New Jersey 08544, USA*

⁴ *Quantum Matter Institute, University of British Columbia, Vancouver, BC V6T 1Z4, Canada*

⁵ *Department of Physics & Astronomy, University of British Columbia, Vancouver, BC V6T 1Z1, Canada*

⁶ *Centre Énergie Matériaux Télécommunications, Institut National de la Recherche Scientifique, Varennes, Québec J3X 1S2, Canada*

⁷ *Nanoelectronics Research Institute, National Institute of Advanced Industrial Science and Technology, Tsukuba, Ibaraki 305-8568, Japan*

⁸ *School of Physics and Astronomy, University of Minnesota, Minneapolis, Minnesota 55455, USA*

⁹ *Dipartimento di Fisica "E.R. Caianiello," Università degli Studi di Salerno, I-84084 Fisciano (SA), Italy*

¹⁰ *CNR-SPIN, UOS di Salerno, I-84084 Fisciano (SA), Italy*

* daniele.fausti@elettra.eu

Superconductivity in the cuprates is characterized by spatial inhomogeneity and an anisotropic electronic gap of d-wave symmetry. The aim of this work is to understand how this anisotropy affects the non-equilibrium electronic response of high-T_c superconductors. We compare the nodal and antinodal non-equilibrium response to photo-excitations with photon energy comparable to the superconducting gap and polarization along the Cu-Cu axis of the sample. The data are supported by an effective d-wave BCS model indicating that the observed enhancement of the superconducting transient signal mostly involves an increase of pair coherence in the antinodal region, which is not induced at the node.

Electronic inhomogeneity [1-10] and anisotropic superconducting (SC) gap in reciprocal space, which features a d-wave symmetry [11-14] are among the most prominent characteristics of the cuprate superconductors. In d-wave superconductors, the electronic transitions at the antinode are limited to frequencies larger than the SC gap, whereas low energy excitations are generally allowed at all frequencies at the node, where the SC gap vanishes. This feature dominates the electronic response and differentiates cuprates from conventional s-wave superconductors [15-19]. We recently reported a marked dependence of the response of cuprate superconductors on the polarization of ultrashort light pulses with photon energies comparable to the antinodal SC gap [20]. We

revealed that mid-Infrared pulses at frequencies comparable to the gap energy and polarized along the Cu-Cu direction drive an enhancement of the SC pairs phase coherence.

Here we study the dynamical response of the electronic excitations and of the SC order parameter arising from different regions of the Fermi surface [21]. By selecting the polarizations of the incoming and the outgoing probe beams, we use time-domain electronic Raman scattering to probe excitations with different symmetries and, thereby, demonstrate that the SC gap exhibits a dynamic response that is different in different parts of the first Brillouin zone. In particular, we study the electronic response of optimally doped

$\text{Bi}_2\text{Sr}_2\text{Y}_{0.08}\text{Ca}_{0.92}\text{Cu}_2\text{O}_{8+6}$ (Y-Bi2212) across the SC transition following a mid-infrared photo-excitation polarized along the Cu-Cu axis and reveal that, whereas antinodal excitations depend strongly on the pump frequency, the nodal ones do not. By rationalizing this experimental evidence through an effective d-wave symmetry BCS model, our findings indicate that low frequency ac-currents along the Cu-Cu direction, driven by long wavelength mid-infrared excitations, may induce a dynamical enhancement of antinodal coherence, possibly also above T_c .

At optimal doping, Y-Bi2212 exhibits a bulk superconductivity below $T_c = 97$ K, a pseudogap phase between T_c and $T^* = 135$ K, a “strange-metallic” phase above T^* [22]. The SC state is characterized by a maximum SC gap amplitude of 2Δ ($T=0$ K) ~ 75 meV [23]. The Bi-based cuprates are prototypical high- T_c superconductors and their phase diagram has been extensively explored via a variety of equilibrium and time-resolved techniques [22-38]. The sample studied here was grown and characterized as described in ref [39]. Y-Bi2212 structure can be approximated by a D_{4h} tetragonal point group and, for parity reasons, the only Raman active modes have A_{1g} , A_{2g} , B_{1g} , B_{2g} and E_g symmetry [40].

In the experimental geometry employed here, where the beam propagation direction is perpendicular to the Cu-O planes, we define the angles α and θ as the polarization directions with respect to the crystallographic Cu-O axis of the input and output probe beams, respectively. In this framework we can express the matrix element of the Raman tensor as

$$R(\alpha, \theta) = \frac{1}{2} [R_{A_{1g}} \cos(\alpha - \theta) + R_{B_{1g}} \cos(\alpha + \theta) + R_{B_{2g}} \sin(\alpha + \theta)] \quad (1)$$

The B modes can be selected through crossed polarization configurations ($\theta = \alpha \pm 90^\circ$), whereas the total symmetric mode A_{1g} cannot be singled out by linearly polarized beams, although its relative high intensity renders all other contributions negligible in parallel polarization measurements ($\alpha = \theta$) [40].

Importantly, by changing Raman scattering configurations, one gains sensitivity to different areas of the reciprocal space: while the B_{1g} configuration selects an area close to the d-wave antinode (Figure 1 c), the B_{2g} symmetry probes the nodal region (Figure 1 e) [20].

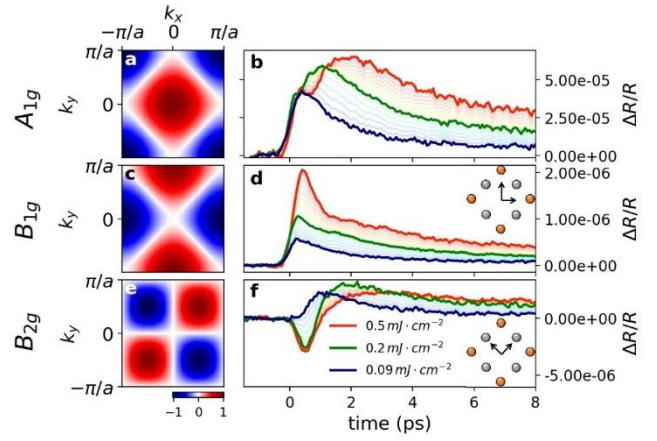


Figure 1: Polarization selection. Left column: sensitivity to the excitations in the first Brillouin zone for different Raman symmetries (a A_{1g} , c B_{2g} and e B_{1g}). Right column: results of the pump-probe experiment at $T=80$ K (below T_c) for different excitation fluence. b No polarization selection (the dominant contribution is A_{1g}), d B_{1g} and f B_{2g} . Three excitation fluences are considered: 0.09 mJ cm^{-2} (blue line) corresponds to the commonly dubbed “linear” response regime, whereas 0.2 mJ cm^{-2} and 0.5 mJ cm^{-2} (green and red line, respectively) refer to the “non-linear” response regime associated to strong perturbation of the SC gap. The inset of panels d and f represent sketches of the Cu-O layer of cuprates (the orange dots represent the Cu atoms and the gray ones the oxygen atoms) and the polarization of the incoming and selected probe beams (arrows).

Figure 1 displays the differential reflectivity probed via ultrashort light pulses centered at 1.63 eV with mid-infrared excitation polarized along the Cu-Cu axis and different incoming and outgoing polarization selections of the probe: (b) polarization integrated measurements, (d) B_{1g} and (f) B_{2g} configurations.

These measurements were performed in the SC phase ($T=80$ K) in different excitation intensity regimes. The low intensity ones (blue lines) are in the “linear” response regime in which the SC order parameter is weakly perturbed. Conversely, higher pump intensities (green and red lines) access the “non-linear” regime where the strong perturbation of the SC phase causes a non-trivial composite response. In the latter case, the observed dip in Fig.1b at ≈ 0.5 ps is usually ascribed to a dynamical melting of the SC phase due to the strength of the photo-excitation [41-45]. Importantly, the time domain response for the different polarization configurations, and consequently for different momentum regions, reveals distinct non-linear dynamical processes: whereas the nodal signal (Fig. 1f) decreases as the pump fluence increases, together with A_{1g} , the response around the antinode (d) survives. Therefore, when the photo-excitation is intense enough to perturb the SC state, beyond the

linear regime, and the negative component appears, the antinodal signal is enhanced (Fig. 1d); Figure 1b is therefore reinterpreted as the result of the composite nodal and antinodal dynamics.

The dynamic response changes at 97 K, when the sample exits the bulk SC phase. Although the temperature dependence of the pump-probe signal has already been investigated in the cuprates [20,40], a study of the mid-infrared electronic dynamics induced for different areas of the Fermi surface is missing. In Figure 2, we show the results of the measurements for B_{1g} and B_{2g} configurations as a function of temperature. Excitations with energy lower than $2|\Delta|$ (where Δ is the gap amplitude at low temperature) and polarization parallel to the Cu-Cu crystallographic direction result in a peculiar gap response: Figure 2 shows the response of the system to excitation with photon energies 170 meV ($>2\Delta$) and 70 meV ($<2\Delta$) and fluence $f=0.09$ mJ cm⁻². The variation of the optical properties of the sample is probed by a near-infrared ($h\nu=1.63$ eV) ultrashort laser pulse.

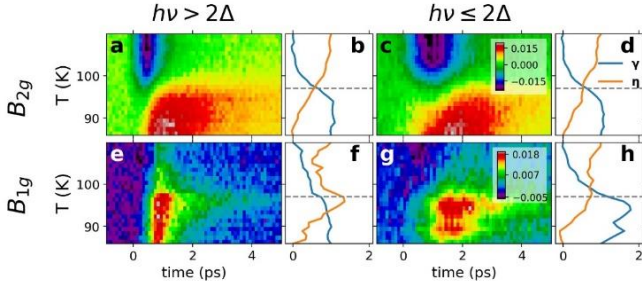


Figure 2: Temperature dependence for different pump photon energies. Temperature-dependent pump-probe measurements, in B_{2g} and B_{1g} configurations, at low fluence (0.09 mJ cm⁻²). Top row: B_{2g} measurements with photo-excitation energies of **a** 170 meV and **c** 70 meV. Panels **b** and **d** display the values of $\gamma(T)$ and $\eta(T)$ (Eq. 2) obtained from the data in **a** and **c**, respectively. The dashed grey lines highlight the critical temperature T_c . Bottom row (Figs. **e-h**): same analysis for measurements in the B_{1g} configuration.

By visual inspection of Figure 2, we note that the “antinodal” (B_{1g}) temperature maps (panels **e** and **g**) strongly depend on the pump photon energy, whereas the “nodal” (B_{2g}) ones show no significant difference (panels **a** and **c**). In order to qualitatively quantify this difference, we fit the signal at a fixed temperature to a linear combination of a SC and a pseudogap time-resolved signal, as described by the relation

$$f(T) = \gamma(T)S_{SC} + \eta(T)S_{PG} \quad (2)$$

where $f(T)$ is the pump-probe signal at temperature T , and $S_{SC}=f(T=85$ K) and $S_{PG}=f(T=110$ K) are the signal measured below and above the critical temperature, respectively. In this way, the coefficients $\gamma(T)$ and $\eta(T)$ effectively weight the contributions of the superconducting and pseudogap signals to the response at a given temperature T . We stress that the qualitative results discussed here do not depend on the arbitrarily chosen temperature (as long as they are well within the two phases) and that this procedure does not aim at identifying T_c , but it is rather used to obtain a qualitative criterion to compare the response at different wavelength for the two polarization configurations (see supplemental materials for details). The results of this procedure are displayed in Fig. 2 **b, d, f, h**.

In spite of the qualitative nature of this analysis, the temperature dependence of $\gamma(T)$ and $\eta(T)$ captures the transition between the signals coming from SC and the pseudogap phases and the curves of the two parameters cross at the critical temperature $T_c=97$ K for “nodal” measurements at low fluence (Figures 2b and d).

Figs. 2 **b** and **d** confirm that the overall transient response in the nodal region of the Brillouin Zone is not affected by the pump photon energy. On the contrary, in the antinodal region (Figures 2 **f** and **h**), the crossing temperature between the fit parameters strongly depends on the photon energy. In particular, for high pump photon energy the pseudogap contribution dominates, whereas for low photon energies the SC contribution prevails for some K above T_c . This reveals that the region in momentum space relevant to the onset of superconducting coherence above T_c is the antinodal one, where the superconducting gap has its maximum value. Analysis for different excitation density (see supplementary) confirm this qualitative response.

In order to rationalize these results, we propose an effective d-wave BCS model interacting with a low-energy pump pulse ($h\nu\sim 2\Delta$) [see [20] for further details and *Supplemental Materials* for the symmetry analysis]. To compare the model with the experimental data, we computed the dynamics of the pair operator expectation value $\psi_{\vec{k}} = \langle \hat{c}_{\uparrow}(\vec{k})\hat{c}_{\downarrow}(-\vec{k}) \rangle$ and tracked the abundance and the coherence of the pairs. In fact, in unconventional superconductors, the transition to the pseudogap phase is not determined by the vanishing of the pairing strength but of phase coherence [43-47]. In particular, we extracted two quantities: λ , the integral over the first Brillouin zone of the pair operator absolute value, which measures the abundance of pairs without considering their mutual and overall d-wave phase coherence, and ϕ , the absolute value of its integral, which measures the abundance of d-wave

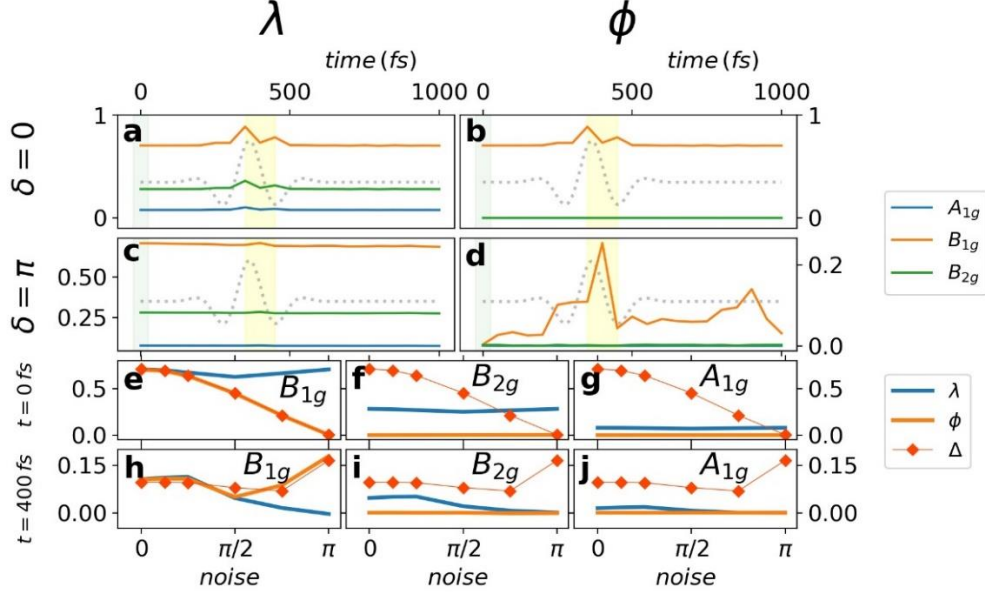


Figure 3: Theoretical Effective model. In **a** and **b**, the dynamics of λ and ϕ (see main text) are displayed. The blue line represents the A_{1g} selection, the orange line the B_{1g} one and the green curve the B_{2g} one. The dashed line shows the time evolution of the pump pulse. In **c** and **d**, random noise with amplitude $\delta = \pi$ was added to the pair operator phase, in order to simulate an initial pseudogap state. In **e-j** the noise dependence of three quantities λ in blue, ϕ in orange and the superconducting gap with the red diamonds) is analyzed for two time delays: at the equilibrium (**e-g**) and immediately after the pump excitation (**h-j**).

coherent pairs. Importantly, the contribution to the electronic response coming from excitation of different symmetry select specific regions (and signs for ϕ) in the Brillouin zone, we computed these quantities by integrating with (the absolute value in the λ case) A_{1g} , B_{1g} or B_{2g} kernels (see Fig 1 a, c and e) and simulate the results of the related symmetry-selective experiments.

The curves in Figure 3a show at time $t=0$ an initial number of pairs that depends on the symmetry selection as well as a time-dependent increase of their number that is correlated with the pump excitation ($t=350$ fs). The calculations reveal an enhancement of the number of pairs much stronger in the antinodal region in agreement with the experiment. A similar dynamical response is shown by the different contributions to the SC gap in Figure 3b, which unveil the prevalent effect of the preservation of the phase coherence over the increase of the number of pairs.

In order to describe the dynamical response above T_C , we propose to modify the equilibrium state of the BCS superconductor by introducing “artificially” phase incoherence, which could effectively mimic the presence of inhomogeneities in the system. This choice is justified by the evidence that in this temperature

range SC fluctuations may persist, while macroscopic superconducting coherence is lost [46-53], likely because different spatial regions of the material can exhibit different pair phases [2,4,15]. In the calculations, we add a uniform random noise to the phase of the expectation value of the pair operator [20]. The dependence of the amplitude of the SC gap on the noise amplitude δ is shown in Fig. 3e (red diamonds), where the noise increase determines the complete collapse of the superconducting gap (for $\delta=\pi$), despite the presence of pairs. Fig. 3 e-g show also that at the equilibrium the dominant contribution to the gap amplitude comes from the antinodal region (orange line in Fig. 3e) for any coherence condition.

By considering this initial arbitrary state with maximum incoherence ($\delta=\pi$) and letting it evolve through our modified BCS Hamiltonian, we obtain the dynamical response for the different symmetries shown in Fig. 3 c-d. In this scenario, the pairs’ abundance is much less affected by the pump excitation for any geometry (Fig. 3 c). On the contrary, a different behavior is observed for the SC gap: in the B_{2g} and A_{1g} configurations we observe a negligible modification of the gap induced by the pump, whereas the B_{1g} contribution from the initial zero value ($t=0$ fs) increases sharply around $t=300$ fs (Fig. 3 c). These results suggest that a low photon energy excitation is

able to dynamically restore phase coherence in the antinodal region of the system.

In conclusion, we studied the dynamical response of electronic excitations in optimally doped Y-B2212. By properly combining the polarization of the incoming and scattered probe beam, we were able to isolate the contributions to the pump wavelength dependence of the SC response observed in [20], coming from different regions of the Fermi Surface. In contrast to the nodal signal, the response at the antinodes is strongly dependent on the pump photon energy, while the nodal is not. More specifically, our results indicate that low photon energy excitations polarized along the Cu-Cu direction affect the of Cooper pairs density only slightly (and do not above T_c), but they dynamically induce pair coherence in the antinodal region (both above and below T_c). In the presence of an inhomogeneous system above T_c , this could give rise to a non-zero superconducting gap and superconducting-like behaviors, which might contribute to the observed light-driven coherent transport above T_c [54-61]. Finally, we stress that the possibility to enhance d-wave phase coherence at the antinodes through driven

currents in the Cu-Cu direction may be of relevance for understanding both equilibrium and non-equilibrium properties of unconventional superconductors.

Acknowledgments This work was mainly supported by the European Commission through the ERCStG2015, INCEPT, Grant No. 677488. This research was undertaken thanks in part to funding from the Max Planck UBC Centre for Quantum Materials and the Canada First Research Excellence Fund, Quantum Materials and Future Technologies Program. The work at UBC was supported by the Killam, Alfred P. Sloan, and Natural Sciences and Engineering Research Council of Canada (NSERC) Steacie Memorial Fellowships (A.D.), the Alexander von Humboldt Fellowship (A.D.), the Canada Research Chairs Program (A.D.), NSERC, Canada Foundation for Innovation (CFI) and CIFAR Quantum Materials Program. The work at the University of Minnesota was funded by the Department of Energy through the University of Minnesota Center for Quantum Materials under DE-SC-0016371. A. A. acknowledges support by MIUR under Project PRIN 2017RKWTMY

References

- [1] J. W. Alldredge, K. Fujita, H. Eisaki, S. Uchida and Kyle McElroy, *Universal disorder in $Bi_2Sr_2CaCu_2O_{8+x}$* , Phys. Rev. B 87, 104520 (2013)
- [2] D. Pelc, Z. Anderson, B. Yu, C. Leighton, M. Greven, *Universal superconducting precursor in three classes of unconventional superconductors*, Nature Communications, 10, 2729 (2019)
- [3] D. Pelc, M. Vučković, M. S. Grbić, M. Požek, G. Yu, T. Sasagawa, M. Greven, Neven Barišić, *Emergence of superconductivity in the cuprates via a universal percolation process*, Nature Communication 9, 4327 (2018)
- [4] P. Popčević, D. Pelc, Y. Tang, K. Velebit, Z. Anderson, V. Nagarajan, G. Yu, M. Požek, N. Barišić, M. Greven, *Percolative nature of the direct-current paraconductivity in cuprate superconductors*, Quantum Materials 3, 42 (2018)
- [5] D. Pelc, P. Popčević, M. Požek, M. Greven and N. Barišić, *Unusual behavior of cuprates explained by heterogeneous charge localization*, Science Advances, 5, 1, eaau4538 (2019)
- [6] P. M. Singer, A. W. Hunt, and T. Imai, *^{63}Cu NQR Evidence for Spatial Variation of Hole Concentration in $La_{2-x}Sr_xCuO_4$* Phys. Rev. Lett., 88, 4 (2002)
- [7] J. Bobroff, H. Alloul, S. Ouazi, P. Mendels, A. Mahajan, N. Blanchard, G. Collin, V. Guillen, and J.-F. Marucco, *Absence of Static Phase Separation in the High T_c Cuprate $YBa_2Cu_3O_{6+y}$* , Phys. Rev. Lett., 89, 15 (2002)
- [8] J. C. Phillips, A. Saxena, A.R. Bishop, *Pseudogaps, dopants, and strong disorder in cuprate high-temperature superconductors*. Rep. Prog. Phys. 66, 2111–2182 (2003)
- [9] Ø. Fischer, M. Kugler, I. Maggio-Aprile, C. Berthod, and C. Renner, *Scanning tunneling spectroscopy of high-temperature superconductors*, Rev. Mod. Phys., 79, (2007)
- [10] G. Yu, D.-D. Xia, D. Pelc, R.-H. He, N.-H. Kaneko, T. Sasagawa, Y. Li, X. Zhao, N. Barišić, A. Shekhter, and M. Greven, *Universal precursor of superconductivity in the cuprates*, Phys. Rev. B 99, 214502 (2019)
- [11] D. J. Scalapino, E. Loh, Jr., and J. E. Hirsch. *d-wave pairing near a spin-density-wave instability*, Phys. Rev. B, 34, 11 (1986)
- [12] P. Monthoux et al., Phys. Rev. Lett., 67, 24 (1991)

- [13] P. Monthoux, A. V. Balatsky, and D. Pines, *Toward a theory of high-temperature superconductivity in the antiferromagnetically correlated cuprate oxides*, Phys. Rev. Lett. 72, 396 (1994)
- [14] T. P. Devereaux and D. Einzel, *Electronic Raman scattering in superconductors as a probe of anisotropic electron pairing*, Phys. Rev. B, 51, 22, (1995)
- [15] F. Cilento et al., *Photo-enhanced antinodal conductivity in the pseudogap state of high-Tc cuprates*, Nature Communications 5, 4353 (2014)
- [16] E. J. Nicol and J. P. Carbotte, *Comparison of s- and d-wave gap symmetry in nonequilibrium superconductivity*, Phys. Rev. B 67, 214506 (2003)
- [17] V. V. Kabanov, J. Demsar, B. Podobnik, and D. Mihailovic, *Quasiparticle relaxation dynamics in superconductors with different gap structures: Theory and experiments on $YBa_2Cu_3O_{7-\delta}$* , Phys. Rev. B 59, 2, (1999)
- [18] R. Cortés, L. Rettig, Y. Yoshida, H. Eisaki, M. Wolf, and U. Bovensiepen, *Momentum-Resolved Ultrafast Electron Dynamics in Superconducting $Bi_2Sr_2CaCu_2O_{8+\delta}$* , Phys. Rev. Lett. 107, 097002 (2011)
- [19] C. L. Smallwood, J. P. Hinton, C. J. Wentao Zhang, J. D. Koralek, H. Eisaki, D.-H. Lee, J. Orenstein, A. Lanzara, *Tracking Cooper pairs in a cuprate superconductor by ultrafast angle-resolved photoemission* Science, 336, 6085, 1137-1139 (2012)
- [20] F. Giusti, A. Marciniak, F. Randi, G. Sparapassi, F. Boschini, H. Eisaki, M. Greven, A. Damascelli, A. Avella, and D. Fausti, *Signatures of Enhanced Superconducting Phase Coherence in Optimally Doped $Bi_2Sr_2Y_{0.08}Ca_{0.92}Cu_2O_{8+\delta}$ Driven by Midinfrared Pulse Excitations* Phys. Rev. Lett. 122, 067002 (2019)
- [21] T. P. Devereaux and R. Hackl, *Inelastic light scattering from correlated electrons* Rev. Mod. Phys. 79, 175 (2007)
- [22] F. Cilento, S Dal Conte, G Coslovich, F Banfi, G Ferrini, H. Eisaki, M Greven, A Damascelli,, D van der Marel, F Parmigiani and C Giannetti, *In search for the pairing glue in cuprates by non-equilibrium optical spectroscopy*. J. Phys.: Conf. Ser. 449, 012003 (2013)
- [23] W. S. Lee I. M. Vishik, K. Tanaka, D. H. Lu, T. Sasagawa, N. Nagaosa, T. P. Devereaux, Z. Hussain, Z.-X. Shen, *Abrupt onset of a second energy gap at the superconducting transition of underdoped Bi_2212* , Nature 450, 81-84 (2007)
- [24] D. N. Basov, T. Timusk, *Electrodynamics of high-Tc superconductors*, Rev. Mod. Phys. 77, 721 (2005).
- [25] H. J. A. Molegraaf, C. Presura, D. van der Marel, P. H. Kes, M. Li, *Superconductivity-Induced Transfer of In-Plane Spectral Weight in $Bi_2Sr_2CaCu_2O_{8+\delta}$* , Science 295, 2239–2241 (2002)
- [26] C. Giannetti, et al., *Revealing the high-energy electronic excitations underlying the onset of high-temperature superconductivity in cuprates*, Nature Communications 2, 353 (2011)
- [27] L. Li, Y. Wang, S. Komiya, S. Ono, Y. Ando, G. D. Gu, and N. P. Ong, *Diamagnetism and Cooper pairing above T_c in cuprates* Phys. Rev B 81, 054510 (2010)
- [28] R. A. Kaindl, M. A. Carnahan, D. S. Chemla, S. Oh, and J. N. Eckstein, *Dynamics of Cooper pair formation in $Bi_2Sr_2CaCu_2O_{8+\delta}$* , Phys. Rev B 72, 060510 (2005)
- [29] M. P. A. Fisher and D. H. Lee *Phys. Correspondence between two-dimensional bosons and a bulk superconductor in a magnetic field*, Rev B, 39, 1 (1989)
- [30] Y. Hwu, L. Lozzi, M. Marsi, S. La Rosa, M. Winokur, P. Davis, M. Onellion, H. Berger, F. Gozzo, F. Lévy, and G. Margaritondo, *Electronic spectrum of the high-temperature superconducting state*, Phys. Rev. Lett., 67, 2573 (1991)
- [31] H. Anzai, A. Ino, M. Arita, H. Namatame, M. Taniguchi, M. Ishikado, K. Fujita, S. Ishida & S. Uchida, *Relation between the nodal and antinodal gap and critical temperature in superconducting Bi_2212* , Nature Communications 4:1815 (2013)
- [32] E. Schachinger and J. P. Carbotte, *Coupling to spin fluctuations from conductivity scattering rates*, Phys. Rev B, 62, 13 (2000)
- [33] W. Zhang, C. L. Smallwood, C. Jozwiak, T. L. Miller, Y. Yoshida, H. Eisaki, D.-H. Lee, and A. Lanzara, *Signatures of superconductivity and pseudogap formation in nonequilibrium nodal quasiparticles revealed by ultrafast angle-resolved photoemission*, Phys. Rev B 88, 245132 (2013)

- [34] G. Coslovich, C. Giannetti, F. Cilento, S. Dal Conte, T. Abebaw, D. Bossini, G. Ferrini, H. Eisaki, M. Greven, A. Damascelli, and F. Parmigiani, Competition Between the Pseudogap and Superconducting States of $\text{Bi}_2\text{Sr}_2\text{Ca}_{0.92}\text{Y}_{0.08}\text{Cu}_2\text{O}_{8+\delta}$ Single Crystals Revealed by Ultrafast Broadband Optical Reflectivity, *Phys. Rev. Lett.* 110, 107003 (2013)
- [35] Fong Liu and Gene F. Mazenko, *Growth kinetics of systems with continuous symmetry*, *Phys Rev B* 45, 6989 (1992)
- [36] C Giannetti, M Capone, D Fausti, M Fabrizio, F Parmigiani, D Mihailovic, *Ultrafast optical spectroscopy of strongly correlated materials and high-temperature superconductors: a non-equilibrium approach*, *Advances in Physics* 65:2, 58-238 (2016)
- [37] J. Yang, PhD thesis. University of Colorado, Boulder, 2017
- [38] C. Thomsen and G. Kaczmarczyk, from *Handbook of Vibrational Spectroscopy* (2002)
- [39] H. Eisaki, N. Kaneko, D. L. Feng, A. Damascelli, P. K. Mang, K. M. Shen, Z.-X. Shen, and M. Greven, *Effect of chemical inhomogeneity in bismuth-based copper oxide superconductors*, *Phys. Rev. B* 69, 064512 (2004)
- [40] Y. Toda, F. Kawanokami, T. Kurosawa, M. Oda, I. Madan, T. Mertelj, V. V. Kabanov, and D. Mihailovic, Rotational symmetry breaking in $\text{Bi}_2\text{Sr}_2\text{CaCu}_2\text{O}_{8+\delta}$ probed by polarized femtosecond spectroscopy, *Phys. Rev. B* 90, 094513 (2014)
- [41] I. Madan, T. Kurosawa, Y. Toda, M. Oda, T. Mertelj, P. Kusar, D. Mihailovic, *Separating pairing from quantum phase coherence dynamics above the superconducting transition by femtosecond spectroscopy*, *Scientific Report*, 4, 5656 (2014)
- [42] P. Kusar, V. V. Kabanov, J. Demsar, T. Mertelj, S. Sugai, and D. Mihailovic, *Controlled Vaporization of the Superconducting Condensate in Cuprate Superconductors by Femtosecond Photoexcitation*, *Phys. Rev. Lett.*, 101, 227001 (2008)
- [43] L. R. Testardi, *Destruction of Superconductivity by Laser Light*, *Phys. Rev. B*, 4, 2189 (1971)
- [44] C. Giannetti, G. Coslovich, F. Cilento, G. Ferrini, H. Eisaki, N. Kaneko, M. Greven, and F. Parmigiani, *Discontinuity of the ultrafast electronic response of underdoped superconducting $\text{Bi}_2\text{Sr}_2\text{CaCu}_2\text{O}_{8+\delta}$ strongly excited by ultrashort light pulses*, *Phys. Rev. B* 79, 224502 (2009)
- [45] L. Stojchevska, P. Kusar, T. Mertelj, V. V. Kabanov, Y. Toda, X. Yao, and D. Mihailovic, *Mechanisms of nonthermal destruction of the superconducting state and melting of the charge-density-wave state by femtosecond laser pulses*, *Phys. Rev. B* 84, 180507 (2011)
- [46] L. Perfetti, B. Sciolla, G. Biroli, C. J. van der Beek, C. Piovera, M. Wolf, and T. Kampfrath, *Ultrafast Dynamics of Fluctuations in High-Temperature Superconductors Far from Equilibrium*, *Phys Rev Lett.* 114, 067003 (2015)
- [47] J. Corson, R. Mallozzi, J. Orenstein, J. N. Eckstein, I. Bozovic *Vanishing of phase coherence in underdoped $\text{Bi}_2\text{Sr}_2\text{CaCu}_2\text{O}_{8+\delta}$* , *Nature* 398, 221 (1999)
- [48] F. Boschini et al., *Collapse of superconductivity in cuprates via ultrafast quenching of phase coherence*, *Nature Materials* 17, 416-420 (2018)
- [49] Kondo, T., Malaeb, W., Ishida, Y. et al. Point nodes persisting far beyond T_c in $\text{Bi}2212$, *Nature Communication* 6, 7699 (2015)
- [50] M. S. Grbić, N. Barišić, A. Dulčić, I. Kupčić, Y. Li, X. Zhao, G. Yu, M. Dressel, M. Greven, and M. Požek, *Microwave measurements of the in-plane and c-axis conductivity in $\text{HgBa}_2\text{CuO}_{4+\delta}$: Discriminating between superconducting fluctuations and pseudogap effects*, *Phys. Rev. B* 80, 094511 (2009)
- [51] L. Bilbro,, R. Aguilar, G. Logvenov, O. Pelleg, I. Božović, N. P. Armitage *Temporal correlations of superconductivity above the transition temperature in $\text{La}_{2-x}\text{Sr}_x\text{CuO}_4$ probed by terahertz spectroscopy*, *Nature Phys* 7, 298–302 (2011)
- [52] J. Orenstein, J. Corson, S. Oh, J.N. Eckstein, *Superconducting fluctuations in $\text{Bi}_2\text{Sr}_2\text{Ca}_{1-x}\text{Dy}_x\text{Cu}_2\text{O}_{8+\delta}$ as seen by terahertz spectroscopy*, *Ann. Phys.* 15, 596{605 (2006)
- [53] I. Kokanović, D. J. Hills, M. L. Sutherland, R. Liang, and J. R. Cooper, *Diamagnetism of $\text{YBa}_2\text{Cu}_3\text{O}_{6+x}$ crystals above T_c : Evidence for Gaussian fluctuations*, *Phys. Rev. B* 88, 060505(R) (2013)
- [54] D. Fausti, R. I. Tobey, N. Dean, S. Kaiser, A. Dienst, M. C. Hoffmann, S. Pyon, T. Takayama, H. Takagi, A. Cavalleri *Light-*

- Induced Superconductivity in a Stripe-Ordered Cuprate.*, Science, 331, 6014-189-191 (2011)
- [55] S. Kaiser, C. R. Hunt, D. Nicoletti, W. Hu, I. Gierz, H. Y. Liu, M. Le Tacon, T. Loew, D. Haug, B. Keimer, and A. Cavalleri, *Optically induced coherent transport far above T_c in underdoped $YBa_2Cu_3O_{6+\delta}$* Phys. Rev. B 89, 184516 (2014)
- [56] W. Hu, S. Kaiser, D. Nicoletti, C. R. Hunt, I. Gierz, M. C. Hoffmann, M. Le Tacon, T. Loew, B. Keimer A. Cavalleri, *Optically enhanced coherent transport in $YBa_2Cu_3O_{6.5}$ by ultrafast redistribution of interlayer coupling*, Nature Materials, 13, 705{711 (2014)
- [57] E. Casandruc, D. Nicoletti, S. Rajasekaran, Y. Laplace, V. Khanna, G. D. Gu, J. P. Hill, and A. Cavalleri, *Wavelength-dependent optical enhancement of superconducting interlayer coupling in $La_{1.885}Ba_{0.115}CuO_4$* , Physical Review B, 91, 17 (2015)
- [58] M. Mitrano, A. Cantaluppi, D. Nicoletti, S. Kaiser, A. Perucchi, S. Lupi, P. Di Pietro, D. Pontiroli, M. Riccò, S. R. Clark, D. Jaksch, A. Cavalleri, *Possible light-induced superconductivity in K_3C_{60} at high temperature*, Nature Nature, 530, 461{464 (2016)
- [59] M. Budden et al., Evidence for metastable photo-induced superconductivity in K_3C_{60} arXiv:2002.12835 (2020)
- [60] B. Liu, M. Först, M. Fechner, D. Nicoletti, J. Porras, T. Loew, B. Keimer, and A. Cavalleri, Pump Frequency Resonances for Light-Induced Incipient Superconductivity in $YBa_2Cu_3O_{6.5}$, Phys. Rev X, 10, 011053 (2020)
- [61] J. Tindall, F. Schlawin, M. Buzzi, D. Nicoletti, J. R. Coulthard, H. Gao, A. Cavalleri, M. A. Sentef, D. Jaksch, *Dynamical order and superconductivity in a frustrated many-body system*, arXiv:2005.09073v2 (2020)

Supplemental Material

1. EXPERIMENTAL DESIGN

Laser System

In our experimental set-up the light source is provided by a Light Conversion Pharos Laser, producing 400 $\mu\text{J}/\text{pulse}$ with 1.2 eV photon energy at 50 KHz repetition. It pumps a Non-Collinear Parametric Amplifier (Orpheus-N by Light Conversion) and a Twin Optical Parametric Amplifier (Orpheus TWIN by Light Conversion), which generates the probe and pump pulse respectively.

The optical probe is a 200 fs pulse, tunable in the visible (measurement reported at 1.63 eV). The MIR pump pulses are produced by Difference Frequency Generation (DFG) mixing the signal outputs of the twin OPA.

Sample

The sample is a large and high-quality optimally doped Y-substituted Bi2212 single crystals ($\text{Bi}_2\text{Sr}_2\text{Y}_{0.08}\text{Ca}_{0.92}\text{Cu}_2\text{O}_{8+\delta}$.) grown in an image furnace by the traveling-solvent floating-zone technique with a non-zero Yttrium content, as described in [1]. The sample critical temperature is $T_c=97$ K.

Derivation of the Raman matrix element

In order to derive equation 1, let us consider the Raman tensor of associated to the D_{4h} tetragonal point group. The Raman tensor can be decomposed in the basis of the irreducible representation of the symmetry group of the crystal as

$$R = \sum_n a_n R_{\Gamma_n} \quad (1)$$

where Γ_n is a representation of the symmetry group [2].

For parity reasons, the only Raman active modes of the group are A_{1g} , A_{2g} , B_{1g} , B_{2g} and E_g [3,4] and, considering our experimental geometry, where the beam propagation direction is fixed and perpendicular to the Cu-O plane, the resulting Raman tensor is [4]:

$$R_{B_{12212}} = \frac{1}{2} \begin{bmatrix} R_{A_{1g}} + R_{B_{1g}} & R_{B_{2g}} \\ R_{B_{2g}} & R_{A_{1g}} - R_{B_{1g}} \end{bmatrix} \quad (2)$$

Let us introduce the angles α and θ , which represent the polarization directions with respect to the crystallographic Cu-O axis of the input and output beam respectively; the matrix element of the Raman tensor $R_{\mu\nu}=R(\alpha,\theta)$ is calculated on two states, that is, the incoming beam with polarization $\hat{\epsilon}_I \propto \begin{pmatrix} \cos \alpha \\ \sin \alpha \end{pmatrix}$

and the reflected beam $\hat{\epsilon}_F \propto \begin{pmatrix} \cos \theta \\ \sin \theta \end{pmatrix}$. Applying the two states to the matrix 4, one easily obtains the relation 1.

Detection

Looking at Equation 1, it is clear that the choice of the orthogonal angles α and θ is not the only way to obtain B_{1g} and B_{2g} dynamics. As a matter of fact, the subtraction of two signals with orthogonal θ angles can produce the same result. For example, for $\alpha=0^\circ$ and $\theta_{1,2}=\pm 45^\circ$ one gets

$$R(\alpha, \theta_{1,2}) = \frac{1}{\sqrt{2}} [R_{A_{1g}} + R_{B_{1g}} \pm R_{B_{2g}}] \quad (3)$$

and so $R(\alpha, \theta_1) - R(\alpha, \theta_2) \propto R_{B_{2g}}$ (see Figure S1 and S2).

Performing the same calculation for $\alpha=45^\circ$, $\theta_1=0^\circ$ and $\theta_2=90^\circ$, one gets $R(\alpha, \theta_1) - R(\alpha, \theta_2) \propto R_{B_{1g}}$.

This demonstrates that birefringent measurements, i.e. the detection of the difference between two orthogonal components of the probe pulses, with suitable angles can represent an alternative technique to acquire B_{1g} and B_{2g} signals, as illustrated in Figure S1. In order to check the validity of the alternative method, in Figure S2 we compare the B_{2g} dynamics measured with the two techniques: the orange line is obtained with the standard configuration ($\alpha=0^\circ$ and $\theta=90^\circ$) whereas the black one refers to the birefringence measurement. The two signals are proportional both in the superconducting phase (Figure S2 a and c) and in pseudogap (Figure S2 b and d) and in the two fluence regimes (linear: Figure S2 a and b, non-linear: c - d).

The measurement of the birefringence is particularly convenient because the cross polarization measurements needed to select B_{1g} and B_{2g} signals can be disturbed by A_{1g} contributions, often present because of the high intensity of the total symmetric signal with respect to the others. On the contrary, in a birefringence measurement the A_{1g} component is split in two contributions, which are equal if the polarization angles $\theta_{1,2}$ are symmetric with respect to the probe polarization α . The final subtraction cancels completely the total symmetric contribution.

So, we performed birefringence time resolved measurements with suitable input and output polarization directions ($(\alpha, \theta_{1,2}) = (0^\circ, \pm 45^\circ)$ and $(\alpha, \theta_{1,2}) = (45^\circ, \pm 0 - 90^\circ)$)

The orthogonal polarization components of the probe are split by a Wollaston prism after the interaction with the sample. The final signal is the subtraction of the two projections of the probe beam, performed by a differential photodetector. In the configuration needed to select B_{1g} and B_{2g} symmetries the prism is always oriented such that the measured signal at the equilibrium ($t < 0$) has the same projection on the two axes.

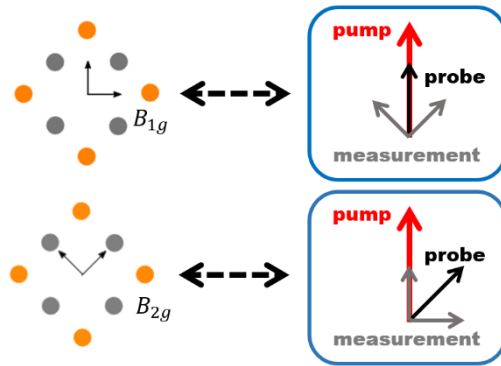


Figure S1: Measurement correspondence. Correspondence between “standard” pump-probe polarization configurations used to measure B_{1g} and B_{2g} signals (on the left) and birefringence measurements (on the right). The colored dots on the left represent the copper (orange) and oxygen (grey) atoms, whereas the arrows show the polarization of the incoming probe beam and the polarization selection after the sample. On the right panel the polarizations of the birefringence measurement are shown: the black line represents the incoming probe and the grey ones the two final polarization selections after the sample.

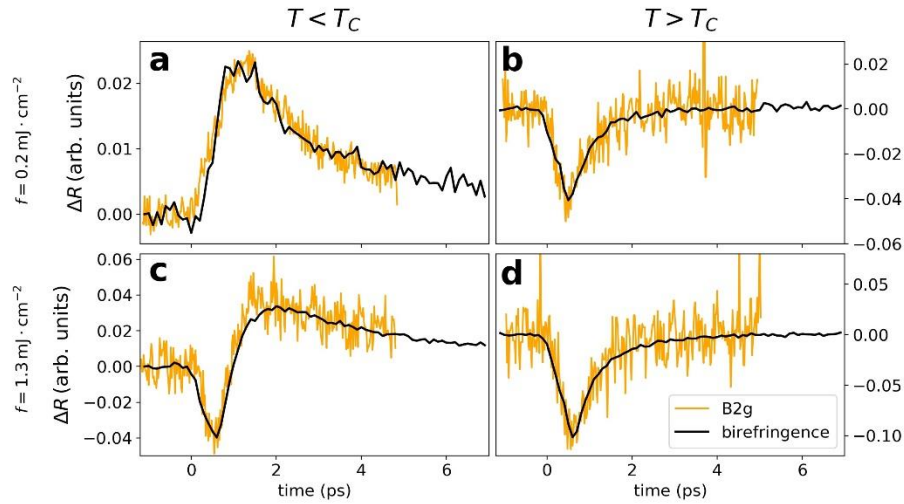


Figure S2: Measurement comparison. Comparison between a pump probe measurement performed in B_{2g} configuration (orange line) and a birefringence measurement (black line, obtained by subtracting the polarization components along the Cu-Cu axes), both in superconducting phase (a and c) and in pseudogap (b and d). The measurements have been performed in two different pump fluence regimes (0.2 mJ/cm² in a and b and 1.3 mJ/cm² in c and d). The signals have been rescaled in order to verify the proportionality between the two measurements.

2. FITTING PROCEDURE

In order to check the validity of the fitting procedure described in the main text (Equation 2), here we analyze the results obtained for higher fluence excitations and finally compare the measured data with the results of the fit.

High fluence measurements

Figure S3 shows the temperature maps of the pump-probe measurements in which the sample is excited with higher fluence pulses ($f = 0.4 \text{ mJ} \cdot \text{cm}^{-2}$), in order to check the temperature dependence of the parameters A and B of the fitting procedure. In particular, the results reported in Figure S3 b, d, f and h suggest that the crossing between the two parameters, which should occur at the transition temperature in our interpretation, is shifted to lower temperatures with respect to the low fluence measurements reported in the main text. We interpret this behavior as the result of the strong non-linear excitation produced by the pump pulse, which is able to dynamically perturb (or even destroy) the superconducting phase, resulting in an effective decrease of the measured T_c . Interestingly, the effect is much more visible when we select the response of the antinodal region (B_{1g} configuration, Figure S3 f and h), where the SC gap has its maximum value at the equilibrium, with respect to the nodal one (B_{2g} symmetry, Figure S3 b and d).

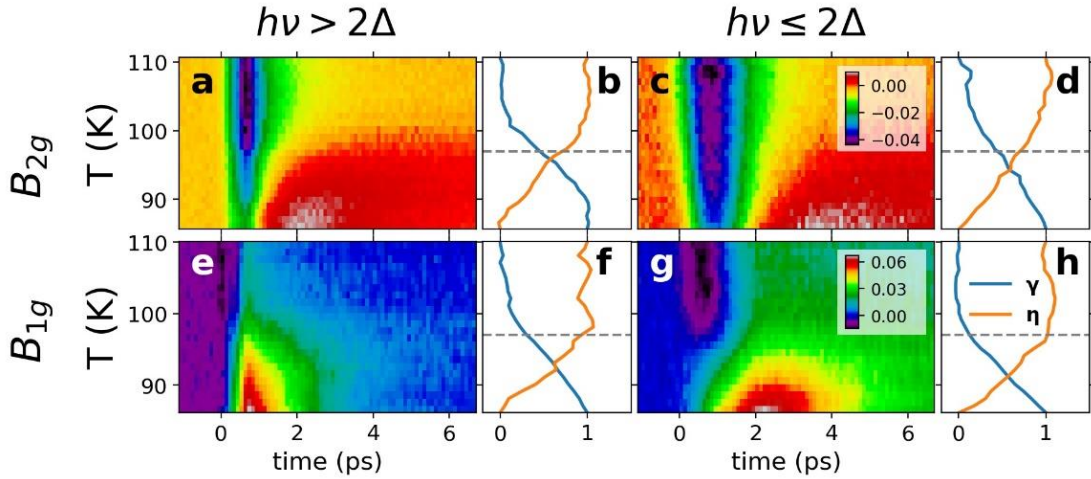


Figure S3: High fluence measurements. Temperature-dependent pump-probe measurements, in B_{2g} and B_{1g} configurations, with high fluence excitations (0.4 mJ cm^{-2}). First row: B_{2g} measurements with different excitation photon energies (**a** 170 meV and **c** 70 meV). The graphs **b** and **d** display the values of $\gamma(T)$ and $\eta(T)$ (Eq. 6) obtained from the data in **a** and **c**, respectively. The dashed grey lines represent the critical temperature T_c . The bottom row (figs. e-h) shows the same analysis for measurements in the B_{1g} configuration.

Results of the fitting procedure

In Figure S4 and S5 we report the complete outcome of the fitting process for nodal (B_{2g}) and antinodal (B_{1g}) response selection respectively, in order to compare the results of the analysis with the linear fit and to check the validity of the procedure.

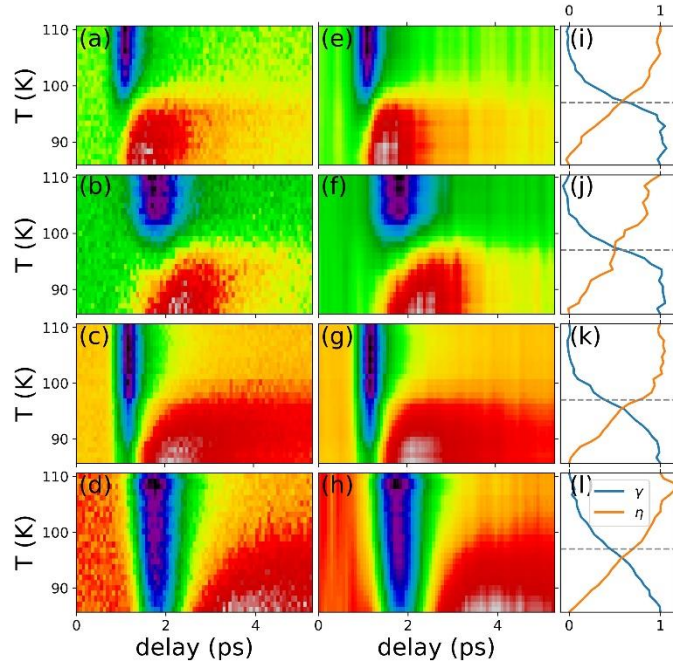


Figure S4: Comparison between data and fit – B_{2g} symmetry. In the left column the measured data are plotted (in the order nodal dynamics for low (a-b) and high (c-d) excitation fluence and high (a, c) and low (b,d) photon energy). In the central column the corresponding fitted maps are shown. The right column displays the values of the fitting parameters γ and η as a function of the temperature. The dashed grey lines represent the critical temperature T_c .

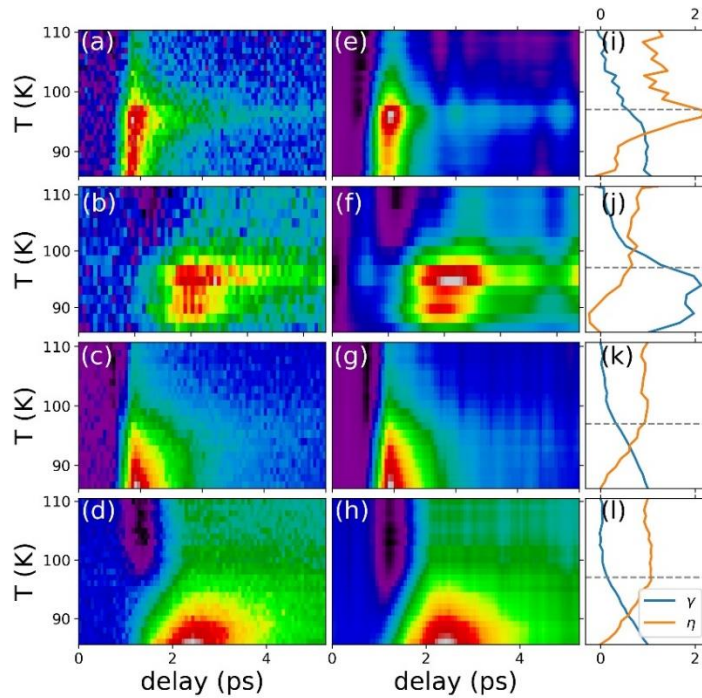


Figure S5: Comparison between data and fit – B_{1g} symmetry. In the left column the measured data are plotted (in the order nodal dynamics for low (a-b) and high (c-d) excitation fluence and high (a, c) and low (b,d) photon energy). In the central column the corresponding fitted maps are shown. The right column displays the values of the fitting parameters γ and η as a function of the temperature. The dashed grey lines represent the critical temperature T_c .

3. BCS EFFECTIVE HAMILTONIAN

In order to interpret the dynamics of the signal, we consider a modified BCS Hamiltonian, which takes into account also the excitation produced by the pump pulse and the anisotropic SC gap, characteristic of high temperature superconductors.

This Hamiltonian can be written as

$$H = \sum_{\vec{k}} \varepsilon \left(\vec{k} - \frac{e}{\hbar} A(t) \vec{\chi} \right) \hat{n}(\vec{k}) + \sum_{\vec{k}} \left(\Delta^*(\vec{k}) \hat{\psi}_{\vec{k}} + \Delta(\vec{k}) \hat{\psi}_{\vec{k}}^+ \right) \quad (4)$$

where $\varepsilon(\vec{k})$ is the two dimensional tight binding electronic dispersion, $A(t)$ is the vector potential of the pump pulse and $\vec{\chi}$ is its polarization. Finally $\Delta(\vec{k})$ is the gap function, whose dependence on \vec{k} remarks its d-wave anisotropy and $\hat{\psi}(\vec{k})$ is the pair operator.

The Hamiltonian is used to calculate the time dependence of the quantity named in the main text, that allows to check the dynamics of the number of Cooper pair and of their phase coherence after the pump excitation. For further details, see [5].

References

- [62] H. Eisaki, N. Kaneko, D. L. Feng, A. Damascelli, P. K. Mang, K. M. Shen, Z.-X. Shen, and M. Greven, *Effect of chemical inhomogeneity in bismuth-based copper oxide superconductors*, Phys. Rev. B 69, 064512 (2004)
- [63] J. Yang, PhD thesis. University of Colorado, Boulder, 2017
- [64] T. P. Devereaux and R. Hackl, *Inelastic light scattering from correlated electrons* Rev. Mod. Phys. 79, 175 (2007)
- [65] Y. Toda, F. Kawanokami, T. Kurosawa, M. Oda, I. Madan, T. Mertelj, V. V. Kabanov, and D. Mihailovic, *Rotational symmetry breaking in $Bi_2Sr_2CaCu_2O_{8+\delta}$ probed by polarized femtosecond spectroscopy*, Phys. Rev. B 90, 094513 (2014)
- [66] F. Giusti, A. Marciniak, F. Randi, G. Sparapassi, F. Boschini, H. Eisaki, M. Greven, A. Damascelli, A. Avella, and D. Fausti, *Signatures of Enhanced Superconducting Phase Coherence in Optimally Doped $Bi_2Sr_2Y_{0.08}Ca_{0.92}Cu_2O_{8+\delta}$ Driven by Midinfrared Pulse Excitations* Phys. Rev. Lett. 122, 067002 (2019)